Jonathan L. Brisman, M.D.
Neurosurgical Service and Epilepsy Research Laboratory, Massachusetts General Hospital, and Harvard Medical School, Boston, Massachusetts

Andrew J. Cole, M.D. F.R.C.P.(C)
Epilepsy Research Laboratory, Massachusetts General Hospital, and Harvard Medical School, Boston, Massachusetts

G. Rees Cosgrove, M.D.
Neurosurgical Service and Epilepsy Research Laboratory, Massachusetts General Hospital, and Harvard Medical School, Boston, Massachusetts

Allan F. Thornton, M.D.
Northeast Proton Beam Regional Therapy Center and Department of Radiation Oncology, Massachusetts General Hospital, and Harvard Medical School, Boston, Massachusetts

Jim Rabinov, M.D.
The NMR Center and Department of Neuroradiology, Massachusetts General Hospital, and Harvard Medical School, Boston, Massachusetts

Marc Bussiere, M.Sc.
Northeast Proton Beam Regional Therapy Center and Department of Radiation Oncology, Massachusetts General Hospital, and Harvard Medical School, Boston, Massachusetts

Maria Bradley-Moore, A.B.
Epilepsy Research Laboratory, Massachusetts General Hospital, and Harvard Medical School, Boston, Massachusetts

Tessa Hedley-Whyte, M.D.
Department of Neuropathology, Massachusetts General Hospital, and Harvard Medical School, Boston, Massachusetts

Paul H. Chapman, M.D.
Neurosurgical Service and Northeast Proton Beam Regional Therapy Center, Massachusetts General Hospital, and Harvard Medical School, Boston, Massachusetts

Reprint requests:
Andrew J. Cole, M.D., Epilepsy Service, Massachusetts General Hospital, VBK 830, 55 Fruit Street, Boston, MA 02114.
Email: cole.andrew@mgh.harvard.edu

Received, April 17, 2002.
Accepted, May 27, 2003.

RADIOSURGERY OF THE RAT HIPPOCAMPUS: MAGNETIC RESONANCE IMAGING, NEUROPHYSIOLOGICAL, HISTOLOGICAL, AND BEHAVIORAL STUDIES

OBJECTIVE: To explore the histological, electrophysiological, radiological, and behavioral effects of radiosurgery using a new model of proton beam radiosurgery (PBR) of the rodent hippocampus.

METHODS: Forty-one rats underwent PBR of the right hippocampus with nominal doses of 5 to 130 cobalt Gray equivalents (CGE). Three control animals were untreated. Three months after PBR, 41 animals were evaluated with the Morris water maze, 23 with T2-weighted magnetic resonance imaging, and 22 with intrahippocampal microelectrode recordings. Animals that were studied physiologically were killed, and their brains were examined with Nissl staining and immunocytochemical staining for glutamic acid decarboxylase, heat shock protein 72 (HSP-72), parvalbumin, calmodulin, calretinin, calbindin, and somatostatin.

RESULTS: Ninety and 130 CGE resulted in decreased performance in the Morris water maze, increased signal on T2-weighted magnetic resonance imaging, diminished granule cell field potentials, and tissue necrosis, which was restricted to the irradiated side. These doses also resulted in ipsilateral up-regulation of calbindin and HSP-72. Parvalbumin was down-regulated at 130 CGE. The 30 and 60 CGE animals displayed a marked increase in HSP-72 staining on the irradiated side but no demonstrable cell loss. No asymmetries were noted in somatostatin, calretinin, and glutamic acid decarboxylase staining. Normal physiology was found in rats receiving up to 60 CGE.

CONCLUSION: This study expands our understanding of the effects of radiosurgery on the mammalian brain. Three months after PBR, the irradiated rat hippocampus demonstrates necrosis at 90 CGE, but not at 60 CGE, with associated abnormalities in magnetic resonance imaging, physiology, and memory testing. HSP-72 was up-regulated at nonnecrotic doses.

KEY WORDS: Behavior, Immunocytochemistry, Magnetic resonance imaging, Neurophysiology, Radiosurgery, Rat

Neurosurgery 53:951-962, 2003 DOI: 10.1227/01.NEU.0000083629.92550.A5 www.neurosurgery-online.com

The use of radiosurgery as a therapy in various central nervous system disorders has grown exponentially in recent years. Indications for radiosurgery, initially used mainly for arteriovenous malformations and tumors, have recently expanded to include functional disorders such as trigeminal neuralgia and epilepsy (15, 37). Experimental studies, however, have lagged behind human clinical trials, and the basic radiobiological effects of focused irradiation on neuronal tissue are still not well understood.

Stereotactic radiosurgery may be performed with the gamma knife, which uses ^{60}Co gamma rays; the linear accelerator (LINAC), which delivers x-rays; or the cyclotron, which uses high-energy protons. Among clinically used radiosurgery devices, only proton beam uses the Bragg peak phenomenon. Protons deposit most of their energy at the Bragg peak, which occurs at the point of greatest penetration of the protons into tissue. In contrast, energy delivered by gamma knife or LINAC decreases exponentially as the particles traverse the tissue. The exact depth to which protons penetrate and at which the Bragg peak occurs is dependent on the energy of the beam. This energy can be precisely

controlled to cause the Bragg peak to fall within a targeted area. Because the protons are absorbed at this point, normal tissue beyond the target receives a minimal dose. Photons of energy emitted by the LINAC or gamma knife do not have the advantage of steep falloff, necessitating the use of multiple sources of energy aligned radially toward a common target (gamma knife) or a multiarc system in which noncoplanar arcs converge on the isocenter (LINAC) to avoid nontarget tissue damage. Protons have an increased ionization density compared with x-rays affecting the prescribed dose. Present practice in proton therapy uses a relative biological effectiveness in the range of 1 to 1.2.

Devices for stereotactic radiosurgery in animal models have been developed, and studies describing basic histological dose response curves have been reported (1, 4, 9, 19–23, 25, 33, 41). However, to better understand the effects of radiosurgery, a more fundamental understanding of the biochemical and electrophysiological changes induced by focused irradiation is needed. For example, although there is evidence from animal and human studies that irradiation in one form or another reduces seizures and alters seizure thresholds, the underlying mechanisms are poorly understood (3, 10, 16, 29, 30, 36, 37, 47, 48).

We therefore sought to investigate the effects of proton beam radiosurgery (PBR) on the normal rat brain. Physiological effects were studied by means of intrahippocampal extracellular microelectrode field recordings from the granule cell layer of the irradiated hippocampus. Behavioral effects were evaluated by the Morris water maze (MWM), a test in which performance is mediated by the hippocampus and is representative of the animal's visuospatial memory capacity. Radiographic effects were studied by measuring signal changes on T2-weighted magnetic resonance imaging (MRI) scans. Last, immunocytochemical studies that used a spectrum of antibodies were performed to test the hypotheses that radiosurgery alters the expression of specific intracellular proteins or selectively affects a subpopulation of cells defined by a specific marker.

MATERIALS AND METHODS

Animal Care

All experiments were conducted in accordance with the guidelines for animal care set forth by the Subcommittee for Research and Animal Care of Massachusetts General Hospital. Rats were housed with a 12-hour light/12-hour dark cycle and provided free access to food and water. Metallic numbered ear tags were used to track animal identity. All animals were male Sprague-Dawley descendent rats (250–350 g; Charles River Breeding Laboratories, Wilmington, MA).

Animal Radiosurgical Device/Stereotactic Radiosurgery

A stereotactic head frame that could be mounted in a clinical beam line at the Harvard Cyclotron Laboratory was developed for proton beam delivery to the right hippocampus of a rat. The head frame was constructed of Lucite and incorporated a bite block and interaural immobilizing bars. We decided that a single dorsal portal would provide the sharpest dose gradient between the right and left hippocampi. The beam line selected for this rodent experiment is routinely used for the treatment of ocular lesions in humans (13) because of its sharp lateral penumbra (80%–20% dose gradient over 1.6 mm) and distal falloff (80%–20% dose gradient over 5.0 mm). By use of rat atlas coordinates (34), a brass aperture was designed to conform to the lateral and longitudinal projections of the right hippocampus. We modeled the hippocampus by means of serial axial sections from the atlas to confirm that the 90% prescription isodose line conformed to its topography in the anteroposterior and dorsoventral dimensions. The aperture dimension included a 2.5-mm margin except along the midline edge, where no margin was added. The 2.5-mm margin is required to allow for a 1.5-mm 90% to 50% penumbra, a 1.0-mm edge definition, and alignment uncertainty. The 90% and 50% values represent the dose prescription level and the dose at the aperture edge, respectively.

The alignment technique used for this experiment relied on projecting a light through the beam-defining aperture onto the exposed rodent skull. The sagittal and coronal sutures and bregma are well defined and provided good alignment references. The medial and anterior aperture edges were placed 0.5 mm from the sagittal suture and anterior to bregma, respectively. Differential doses were administered depending on the treatment protocol.

A computed tomographic scan of a representative rat was obtained by using the stereotactic head frame. The computed tomographic scan allowed the rat atlas dimensions to be confirmed and provided conversion factors for the effective water equivalent depths for the rodent brain and skull. Clinical proton beam penetration is defined as a water equivalent depth. Mapping the hippocampus on the atlas and applying the effective depth conversion factors defined the required proximal (2.3 mm) and distal (5.6 mm) extents to be covered by the prescribed dose (*Fig. 1A*). The measured nonmodulated proton beam with the custom brass aperture had proximal and distal prescription depths of 0.8 and 5.5 mm from the skull, respectively. The surface dose along the portal path was 85% (*Fig. 1, B* and *C*).

Clinical Assessment

The day of irradiation was defined as Day 0. Animals were checked periodically for weight change, spontaneous activity, and neurological impairment. All animals were weighed on Days 23, 40, 48, and 73, and any deviations from expected weight gains were noted. Animals were checked every 4 days for aberrant spontaneous activity within their cages. Animals were formally tested for neurological impairment on Day 73. In this test, the animal was held by the tail, and any abnormal hind limb or forelimb posturing was noted. The animal was then placed on the ground, and any abnormality of gait, limb posturing, or circular movements was noted.

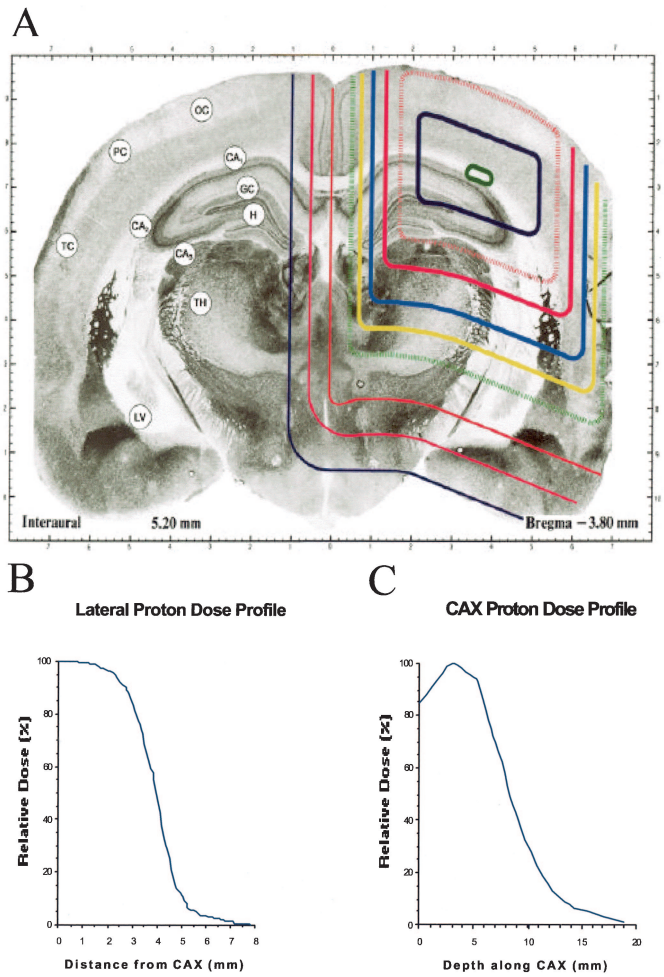

FIGURE 1. *Stereotactic dosimetry planning for unilateral hippocampal proton beam irradiation.* A, *the isodose distribution was overlaid onto a central coronal plane located 3.8 mm posterior to bregma using the Paxinos and Watson stereotactic rat atlas (34). The 90% isodose represents the prescription level and the 50% isodose coincides with the aperture edge. Anatomic regions are indicated on the contralateral hippocampus:* H, *hilus;* GC, *granule cell layer;* CA_3, CA_2, *and* CA_1, *pyramidal cell layers of Ammon's horn;* TH, *thalamus;* LV, *lateral ventricle;* OC, *occipital cortex;* PC, *parietal cortex;* TC, *temporal cortex. The dose profile at the center of the proton Bragg peak along the axis perpendicular to the irradiation beam* (B) *as well as the dose profile along the irradiation beam* (C) *where the 50% isodose line coincides with the aperture edge are displayed.* CAX, *central axis.* Colored lines *indicate isodose lines from innermost* (dark green) *to outermost* (navy blue)*: 100, 95, 90 (prescribed dose), 80, 70, 60, 50, 30, 15, and 8%.*

MWM Testing

A modified MWM was used to assess visuospatial learning and memory. A circular plastic tank (117 cm in diameter) was filled with water to a depth of 25 cm. The water was made opaque by the addition of 100 ml of evaporated milk. The pool was kept in a fixed location throughout the study. Four points on the rim of the pool were designated as north, south, east, and west. On Days 1 through 5, animals were timed in 20 trials, four trials a day, to locate and escape onto a Plexiglas platform (8 × 8 cm) placed 1.5 cm under the water's surface. For each rat, although the quadrant in which the platform was located remained constant, the point of immersion into the pool with the rat held facing the perimeter varied between north, east, south, and west in a random order for the 20 trials. The latency from immersion into the pool to escape onto the platform was recorded. On mounting the platform, the rat was provided a 30-second rest before the next trial. If a rat did not find the platform in 120 seconds, it was manually placed on the platform for a 30-second rest. Final latency, a measure of learning, was calculated as the mean of the fifth day trial subtracted from the mean of the first day trial, divided by the average of the means of the 2 days. A higher score, with a maximal possible score of 2, indicates better visuospatial memory.

Neurophysiological Testing

Twenty-two animals underwent neurophysiological testing 3 months after PBR. Animals were as follows: three control; five receiving 5 cobalt Gray equivalents (CGE); two receiving 12 CGE; one receiving 20 CGE; three receiving 30 CGE; four receiving 60 CGE; three receiving 90 CGE; and one receiving 130 CGE. Animals were anesthetized with urethane (1.25 g/kg subcutaneously) and placed in a Kopf stereotactic device (David Kopf Instruments, Tujunga, CA). Rectal temperature was monitored continuously and maintained at 37 ± 1°C with a heating pad (Harvard Apparatus, Natick, MA). Two holes were drilled in the right side of the animal's skull to accommodate recording and stimulating electrodes. The stimulating electrode (NE-200 bipolar stainless steel electrode; Rhodes Medical Instruments, Woodland Hills, CA), with 0.5-mm tip separation, was placed 4.5 mm lateral to the midline suture and immediately rostral to the lambdoid suture and lowered into the angular bundle of the perforant pathway. The recording electrode (4 mol/L NaCl-filled glass microelectrode, 0.4–1.0 MΩ resistance, 1.5 mm outer diameter) was placed 3.5 mm posterior and 2 mm lateral to bregma and was lowered into the dorsal blade of the granule cell layer (approximately 3.5 mm below the brain surface). Exact placement of the recording electrode was made by optimizing the characteristic shape of the evoked potential. Biphasic current pulses (0.1-ms duration) were generated by a Grass S88 stimulator (Grass Instruments, Quincy, MA) with a Grass stimulus isolation unit. Potentials were amplified by a Grass preamplifier, displayed on a Tektronix (Beaverton, OR) digital oscilloscope, and stored on diskette.

Recordings from the dentate gyrus granule cell layer that uses these stereotactic coordinates revealed a characteristic waveform representing an excitatory postsynaptic potential (EPSP) with a superimposed extracellular granule population spike (*Fig. 2, A–D*). The size of the granule cell spikes on delivering a paired pulse was measured and was provided values, represented as P1 and P2 (*Fig. 2B*, *inset*). The P2/P1

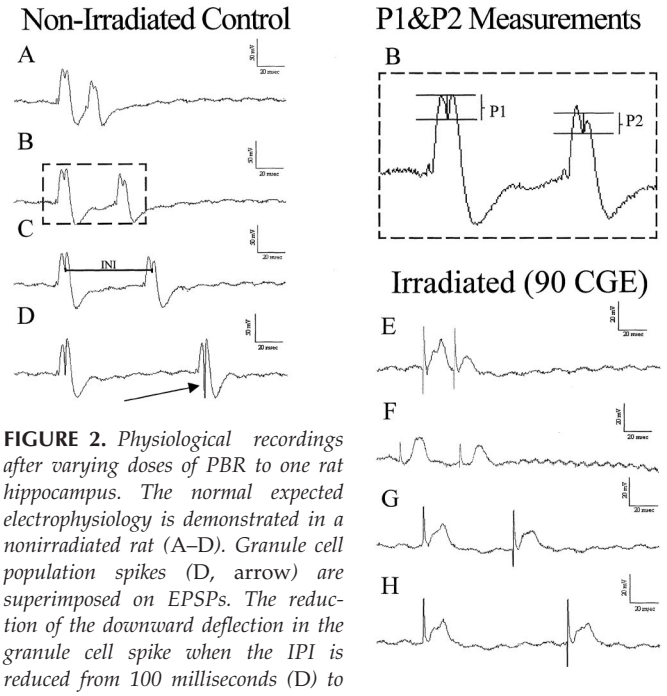

FIGURE 2. *Physiological recordings after varying doses of PBR to one rat hippocampus. The normal expected electrophysiology is demonstrated in a nonirradiated rat (*A–D*). Granule cell population spikes (*D, arrow*) are superimposed on EPSPs. The reduction of the downward deflection in the granule cell spike when the IPI is reduced from 100 milliseconds (*D*) to 60 milliseconds (*C*) to 40 milliseconds (*B*) and ultimately 20 milliseconds (*A*) is a reflection of intact feedback inhibition. P1 and P2 values were measured (*B, inset*). Animals receiving 90 CGE exhibit markedly reduced granule cell population spikes, unaffected by altering the IPI, despite voltages as high as 150 μV (*E–H*). Final EPSPs were diminished in size and were absent until higher than normal voltages were used.*

ratios at various interpulse intervals (IPI) and frequencies were calculated for each animal within each hemisphere of the brain. Ratios were rounded to the nearest whole number. Feedback inhibition was considered present if there was a reduction in the P2/P1 ratio as the IPI was reduced from 100 milliseconds to 20 milliseconds (*Fig. 2, A–D*). Once satisfactory potentials were recorded and inhibition was tested on the irradiated side, or after five failed attempts, the same method of testing was conducted on the contralateral side.

MRI Studies

Twenty-three of the 41 rats were imaged at the 3-month time point. Rats were sedated with intraperitoneally administered pentobarbital (50 mg/kg) and imaged with a standard 1.5-T GE Signa MRI scanner (General Electric, Milwaukee, WI). A 3-inch surface coil was used to obtain 3-mm T1-weighted sagittal images (TR 600 and TE 30) and dual-echo T2-weighted coronal images (TR 3000, TE 30/90). T1-weighted coronal images were also obtained if an abnormality was detected on the T2-weighted images. Off-line volumetric analysis was performed to evaluate areas of increased signal on T2-weighted images. Point-to-point analysis was used to identify areas of 25% signal increase compared with contralateral gray and white matter. This threshold was used to minimize the chance of false-positive interpretations. In some cases, hydrocephalus developed. When it was bilateral, the ventricles were excluded from the volume of parenchymal change. When the hydrocephalus was larger on the irradiated side, only a volume comparable to the untreated left side was excluded. An approximation of the volume of tissue with T2 abnormality was generated for each hippocampal region.

Histological/Immunocytochemical Analysis

Twenty-four hours after neurophysiological testing, animals were killed with pentobarbital (100 mg/kg) and perfusion-fixed transcardially with 4% paraformaldehyde. Brains were stored in situ overnight at 4°C and then harvested, weighed, and cut on a Vibratome (Vibratome Co., St. Louis, MO) in 0.1 mol/L phosphate buffer. Alternate coronal sections (40 μm) were stained with 0.1% cresyl violet, coverslipped, and examined under the light microscope. Additional sections (50 μm) were used for immunocytochemical analyses.

Immunocytochemistry was performed for heat shock protein 72 (HSP-72), somatostatin, glutamic acid decarboxylase 67 (GAD-67), calbindin (CLBD), calmodulin (CLMD), calretinin (CLRT), and parvalbumin (PV). On Day 1, free-floating sections were washed in phosphate-buffered saline, solubilized with 0.3% Triton X-100 in 10% goat serum buffer (G-9023; Sigma Chemical Co., St. Louis, MO), except for GAD-67, and then incubated overnight in primary rabbit polyclonal antibody at 4°C. Primary antibodies were used at the following dilutions: HSP-72 (1:20; Calbiochem, San Diego, CA), somatostatin (1:5000; Incstar Corp., Stillwater, MN), GAD-67 (1:1000; Chemicon, Temecula, CA), CLBD (1:5000; Calbiochem), CLMD (1:100; Zymed Laboratories, South San Francisco, CA), CLRT (1:2000; Research Diagnostics, Flanders, NJ), and PV (1:5000; Calbiochem). On Day 2, sections were again washed in phosphate-buffered saline, then incubated in the secondary antibody overnight at 4°C. Secondary antibody was a biotinylated goat anti-rabbit antibody (Vector Laboratories, Burlingame, CA) prepared in goat serum buffer at 1:200 dilution (biotinylated goat anti-mouse was used for HSP-72). On Day 3, sections were again washed in phosphate-buffered saline and then rinsed for 30 minutes in 0.3% H_2O_2 to quench endogenous peroxidases. Immunoreactivity was then visualized with the three-step avidin-biotin complex technique with diaminobenzidine tetrachloride (with nickel intensification) as substrate (Vectastain Elite; Vector Laboratories). Sections were mounted on slides, counterstained with cresyl violet if the immunocytochemical stain was sufficiently dark to permit it (CLRT, PV), coverslipped, and examined under the light microscope.

Statistical Analysis

MRI volumetrics and brain weights were compared with a single-factor analysis of variance (ANOVA). MWM testing was analyzed with a linear regression line correlating dose with y, where y is the number of successes divided by the total trial time. Significance was defined as $P < 0.05$ for all tests (SAS statistical analysis software; SAS Institute, Cary, NC).

RESULTS

Clinical Evaluation

Three rats that received 20, 130, and 130 CGE developed clinical evidence of neurological dysfunction, and three animals that received 20, 60, and 60 CGE died during the study period. Because the deaths were not detected for several hours, brains could not be analyzed for potential causes of death. All other animals displayed normal behavior during this time period.

MWM Testing

Only two animals, which received 20 and 130 CGE, were unable to perform the MWM. Mean latency for each day of the 5-day trial averaged for each dose of irradiation is plotted graphically in *Figure 3*. A linear regression line correlating dose with the ratio between the number of successes and the total trial time for each animal revealed a statistically significant effect of dose on ability to perform the MWM. Increasing dose of irradiation resulted in poorer performance ($P = 0.0252$). When the higher-dose animals (90 and 130 CGE) were excluded from the analysis, the relation between increasing dose and MWM performance was not statistically significant ($P = 0.8010$).

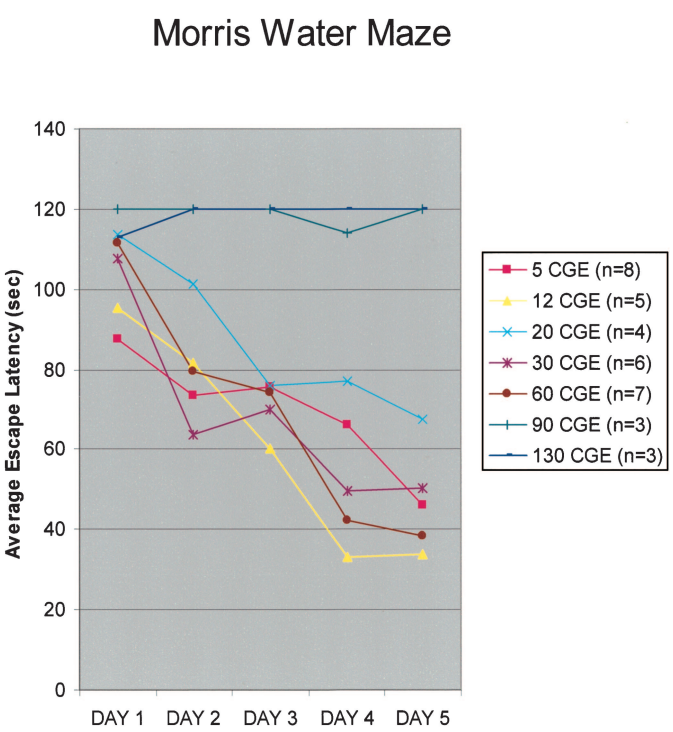

FIGURE 3. *Graphical depiction of MWM acquisition times during a 5-day trial period. All animals except for those receiving 90 or 130 CGE irradiation displayed some degree of learning.*

Neurophysiology

Twenty-two animals were evaluated physiologically. No recognizable potentials were obtainable after five attempts in 13 (4 irradiated, 9 nonirradiated) (30%) of 44 hemispheres in which physiological testing was attempted. In 31 hemispheres, or 70% of attempts, appropriate extracellular field potentials were obtained.

Sixteen of 18 animals receiving less than 90 CGE revealed normal EPSPs and granule cell field potentials with intact recurrent inhibition (*Fig. 2*). Two animals (one control animal and one 30 CGE animal) had only a mild decrease in the P2/P1 ratio with shortening of the IPI, suggesting present but not completely normal recurrent inhibition. Stimulus voltages ranged from 25 to 90 V. No electrical activity was detected in the one animal evaluated physiologically that had received 130 CGE. In animals that had received 90 CGE, all had diminished EPSPs despite an increase of the voltage to 150 V. Two of three animals showed some very small granule cell population spikes without intact inhibition, and in one, no population spikes were evoked (*Fig. 2, E–H*).

MRI Scans

Volumetric analysis of signal changes on MRI scans at 3 months after right hippocampal irradiation is listed in *Table 1*. Mean volumes (mm^3) with an elevation of 25% or more in T2-weighted signal intensity in the right cerebral hemisphere differed significantly between dose groups ($P < 0.001$; ANOVA). Although there was no significant difference between 130 and 90 CGE ($P = 0.32$; ANOVA), brains receiving 90 CGE or more differed significantly from animals receiving 60 CGE or less ($P < 0.001$; ANOVA). In the 130 CGE animals, distortion of normal anatomy and extensive T2-weighted signal abnormality, as shown in *Figure 4*, suggest tissue destruction, although no T1 shortening was observed to indicate methemoglobin. Hydrocephalus was observed in all animals at 130 CGE.

TABLE 1. Magnetic resonance imaging volumetric measurements using T2-weighted imaging after varying doses of proton beam radiosurgery of the rat hippocampus[a]

PBR dose (CGE)	Brain volume of abnormal signal intensity (mm^3)[b]
<60 (n = 13)	0 ± 0.0
60 (n = 3)	24 ± 41.0
90 (n = 3)	322 ± 87.9[c]
130 (n = 4)	495 ± 257.5[c]

[a]PBR, proton beam radiosurgery; CGE, cobalt Gray equivalents.
[b]Numbers refer to computer-generated volumetrics (averaged per group).
[c]$P < 0.001$ when compared with doses of <60 CGE (analysis of variance).

Gross Brain Evaluation

Brain weight ranged from 2.0 to 2.4 g. There was no correlation between weight and irradiation dosage ($P = 0.235$; ANOVA). Two animals (30 and 60 CGE) developed unilateral hydrocephalus on the irradiated side; one had blood in that ventricle, one (90 CGE) had unilateral hydrocephalus on the nonirradiated side, and one (5 CGE) developed bilateral hydrocephalus.

All brains had contusions at the entry site of the four electrodes that were lowered during physiological testing; these consisted of variably sized areas of discoloration and hemorrhage on the dorsal convexity (*Fig. 4, A* and *B*). Brains that received 90 CGE or more had macroscopic evidence of irradiation injury. This injury included a zone of gray discoloration with petechiae on the dorsal convexity (*Fig. 4, A* and *B*) with extension onto the ventral surface of the brain, primarily within the temporal lobe on the irradiated side (130 CGE > 90 CGE, *Fig. 4, D* and *E*). Gross hemorrhagic infarction was also found within the hippocampus in these brains—again, more so in animals at 130 CGE than at 90 CGE (*Fig. 4, G* and *H*). Animals receiving 60 CGE or less showed no gross abnormalities (*Fig. 4, C, F,* and *I*).

Histology (Cresyl Violet)

There were no histological changes detected in animals receiving doses of less than 30 CGE. Two of the three animals receiving 30 CGE and two of the three animals receiving 60 CGE had hippocampal atrophy on the irradiated side when compared with the nonirradiated side. An animal irradiated with 60 CGE with a normal hippocampus examined with Nissl stain is shown in *Figure 5, A* and *B*. Moderate endothelial cell thickening was observed in one animal receiving 30 CGE and one animal receiving 60 CGE, on the irradiated side only. Marked gliosis in the hippocampal fissure was observed on the irradiated side in one of three animals receiving 30 CGE and two of three animals receiving 60 CGE.

Animals receiving 90 CGE or more displayed areas of marked necrosis, edema, inflammatory cells, and neuronal loss, all on the irradiated side (*Fig. 5, C–E*). This damage extended into the surrounding parieto-occipitotemporal neocortex, and to a smaller extent into the underlying caudate putamen and thalamus. Vascular dilation was observed in the hippocampus and underlying structures in the 90 CGE animals. The 130 CGE animal had a necrotic cavity in this area. Damage to the contralateral side was modest (*Fig. 5F*).

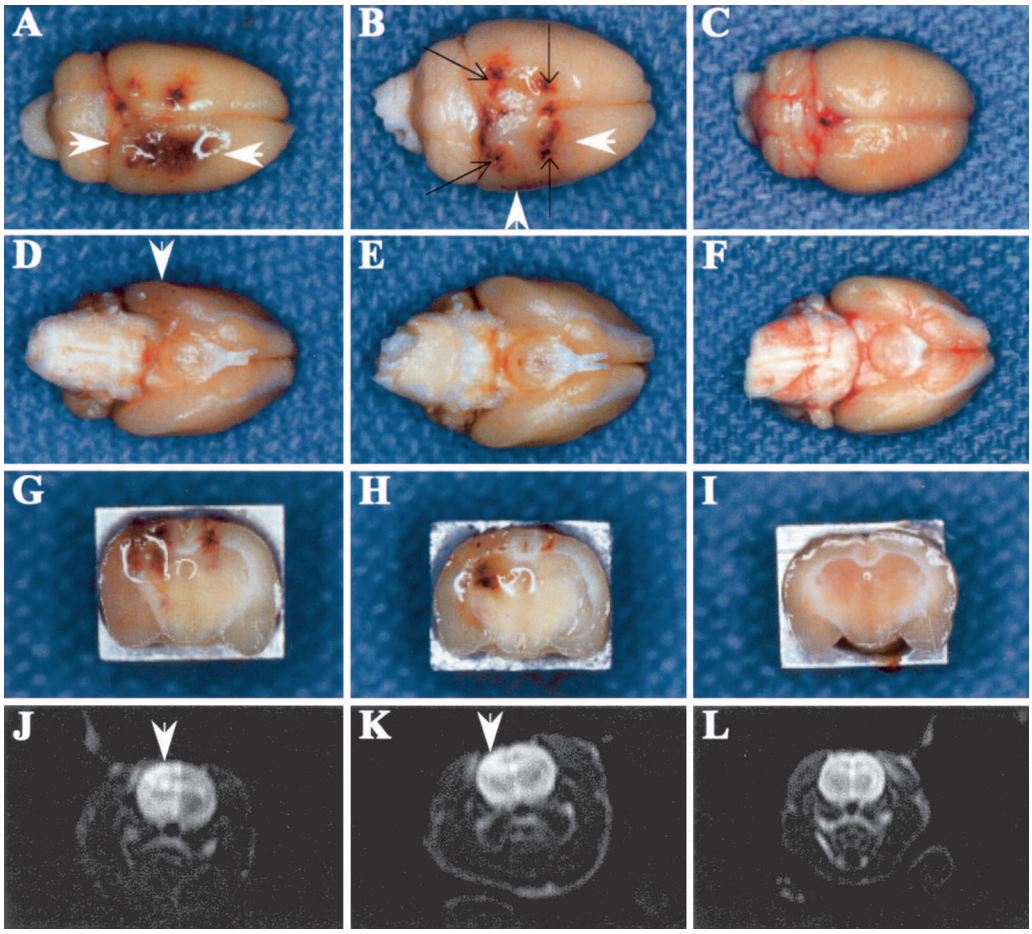

FIGURE 4. *Gross brain anatomy correlated with MRI appearance after 130 CGE* (A, D, G, J)*, 90 CGE* (B, E, H, K)*, or 60 CGE* (C, F, I, L)*, to the right rat hippocampus. Photographs of the whole brain displaying the dorsal* (A–C) *and ventral* (D–F) *surfaces, as well as coronal cut sections* (G–I)*, are shown. Contusions from the stimulating and recording electrodes are seen* (B, black arrows) *and can be reliably differentiated from irradiation-induced damage* (A, B, D, white arrowheads)*. T2-weighted MRI appearance closely parallels the lesions seen on coronal sectioning. Note that 60 CGE animals used for this figure did not have electrodes lowered. No gross or MRI-evident abnormality is present in the 60 CGE animal* (C, F, I, L)*.*

Immunohistochemistry

HSP-72

Cellular staining for HSP-72 was mildly increased in the hippocampus and surrounding cortex at 30 CGE and markedly increased at

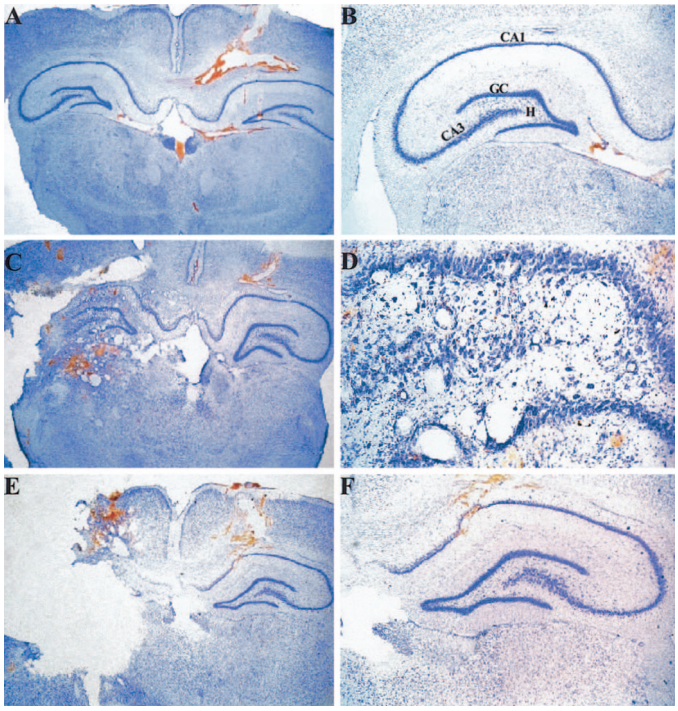

FIGURE 5. *Cresyl violet-stained slides after PBR. Coronal 40-μm whole brain (right side of brain is* left *side of photograph) and hemibrain/hippocampal photomicrographs after 60 CGE (*A *and* B*), 90 CGE (*C *and* D*), and 130 CGE (*E *and* F*). Low-power (*A*, original magnification, ×3.125) and high-power (*B*, original magnification, ×6.25) views of a 60 CGE animal reveal normal histology on both the nonirradiated and irradiated (*B*) sides. Recording electrode tracts are seen extending into left hemisphere (*A*). Low-power view of the 90 CGE brain (*C*, × 3.125) reveals necrosis and tissue loss in both the hippocampus and adjacent cortex with telangiectatic vascular dilation that extends into the thalamus on the irradiated side. Telangiectatic dilation and cellular disorganization and loss are better seen with higher magnification (*D*, ×25). A frank necrotic cavity involving the irradiated hippocampus and cortex is seen in the animal receiving 130 CGE (*E*, original magnification, ×3.125). The nonirradiated side of both the 130 CGE (*F*, original magnification, ×6.25) and 90 CGE (*C*) animals appears relatively normal.* CA_1, CA_3, *pyramidal fields;* GC, *granule cells;* H, *hilus.*

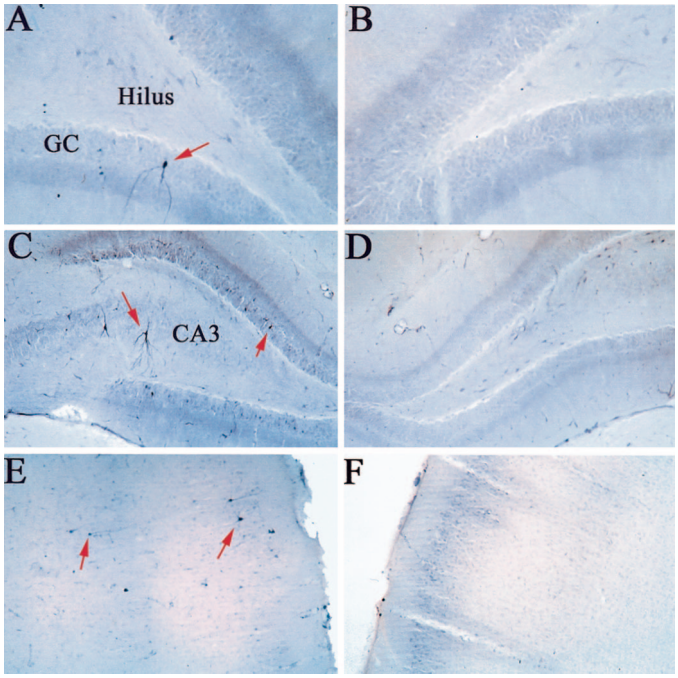

FIGURE 6. *HSP-72 immunocytochemistry in hippocampus and cortex after varying doses of PBR (ipsilateral to irradiation,* A, C, E*; contralateral,* B, D, F*). Cells are stained with HSP-72 in both hippocampus (*A*, 30 CGE, original magnification, ×50; *C*, 60 CGE, original magnification, ×25) and cortex (*E*, 60 CGE, original magnification, ×25) after PBR. Nonirradiated hippocampus (*B*, 30 CGE, original magnification, ×50; *D*, 60 CGE, original magnification, ×25) and cortex (*F*, 60 CGE, original magnification, ×25) have markedly less or no staining. Staining is seen in multiple layers of cortex (*E, red arrows*) as well as in granule cells (*red arrow *in* A *and* short red arrow *in* C*) and CA3 pyramidal neurons (*long red arrow *in* C*) in irradiated animals.* GC, *granule cells (counterstained with cresyl violet).*

doses of 60 CGE or more. Staining was most prominent in the adjacent parieto-occipitotemporal cortex but was found in pyramidal cells of CA1, CA3, the hilus, and granule cells of the hippocampus (*Fig. 6*). This effect was restricted to the irradiated side (*Fig. 6, A, C,* and *E*). At doses of 30 CGE or less, sporadic cells were stained on the irradiated side. At all doses, there were rare cells stained in both the nonirradiated and irradiated hemispheres; no HSP-72 staining was observed in nonirradiated brains.

Calbindin D-$_{28K}$

Animals that received less than 90 CGE did not differ from controls. The 90 CGE animals displayed increased density of cell staining for calbindin D-$_{28K}$ in the granule cell layer and of fiber staining in the inner molecular layer of the irradiated hippocampus. The irradiated cortex in those animals (in addition to that in an animal receiving 130 CGE) revealed increased density of cellular staining and disorganized cellular and fiber architecture (*Fig. 7, A–D*).

Parvalbumin

PV staining in animals that received less than 130 CGE did not differ from controls. One animal that received 130 CGE displayed a noticeable decrease in fiber staining and/or dendritic arborization of stained cells in the irradiated cortex. A decrease in cellular staining in the irradiated cortex was also observed (*Fig. 7, E* and *F*).

CLMD, Somatostatin, GAD-67, and Calretinin

There was no difference among animals in staining for CLMD, somatostatin, GAD-67, or calretinin from the irradiated to the nonirradiated side, nor to the control hippocampi at any irradiation dose.

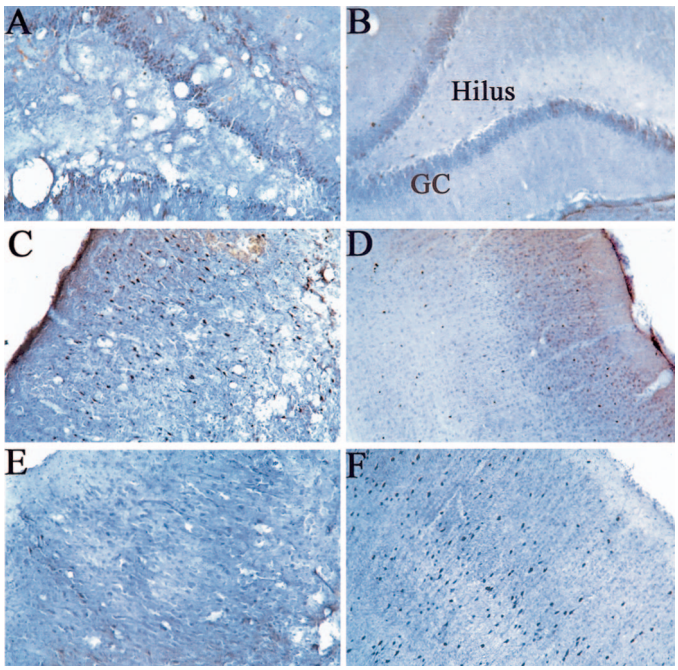

FIGURE 7. *Calbindin D-$_{28K}$ (A–D, 90 CGE) and PV (E and F, 130 CGE) immunoreactivity after varying doses of PBR. Differences between irradiated hippocampus (A) and cortex (C and E) and nonirradiated hippocampus (B) and cortex (D and F) are shown. CLBD is up-regulated in the dentate gyrus granule cells in the irradiated hippocampus and cortex (A, 90 CGE, original magnification, ×25; C, 90 CGE, original magnification, ×25) as compared with the nonirradiated hippocampus and cortex of the same animal (B, 90 CGE, original magnification, ×25; D, 90 CGE, original magnification, ×25). PV is markedly reduced in the irradiated cortex at the highest dose (E, 130 CGE, original magnification, ×25) as compared with the nonirradiated cortex (F, 130 CGE, original magnification, ×25).* GC, *granule cells (counterstained with cresyl violet).*

DISCUSSION

The increasing use of radiosurgery in the human brain, particularly for functional disorders for which traditional treatments are currently effective and low risk, must be accompanied by an increased understanding of the fundamental changes in the brain after such treatment. Although a number of animal experiments have looked at the effects of radiosurgery on the brain (4, 8, 22, 23, 30, 33, 35, 38), several important areas have not been addressed. In this study, we report alterations in neurophysiology, neuronal protein expression, and animal behavior after radiosurgery of one dorsal hippocampus in the rodent. We chose to target the dorsal hippocampus in preparation for future experiments that will attempt to alter the neurophysiological network defect in animals previously rendered epileptic.

MRI

Because MRI is a noninvasive way to monitor the effects of central nervous system irradiation, defining expected MRI responses to varying dosages and post-PBR latencies is important. In particular, we focused on correlating MRI findings with histology and physiology. Interestingly, Regis et al. (37) demonstrated that seizure reduction in humans after radiosurgery correlated with MRI scan changes. Radiosurgery of the hippocampus and entorhinal area with 25 Gy to the 50% isodose line and a total volume of 6500 mm^3 resulted in reproducible MRI changes in five of seven patients at 9 to 10 months, and coincident with cessation of seizure activity. MRI findings included a heterogeneous T2 signal within the hippocampus, which was itself swollen, a contrast-enhancing ring that demarcated the 50% isodose line, and diffusely increased T2 signal within the temporal lobe and adjacent white matter. All abnormal MRI findings resolved by 24 months.

Animal experimentation has included reports on MRI findings after radiosurgery in the rat parietal cortex with the gamma knife (19), in an unspecified target in the rat with LINAC (21), in the rat hemibrain with proton beam (22), and with LINAC in the internal capsule in cats (4). Although one other article reports having performed MRI after radiosurgery of the hippocampus (30), specific results were not provided. We found changes that correlated with necrosis and porencephaly at doses of 90 CGE or more via T2-weighted imaging. Hydrocephalus, when it occurred, was also detected radiographically. MRI alterations were apparent as early as 6 weeks after high doses (data not shown) and after 3 months when 60 CGE was used. MRI changes correlated well with altered physiology, behavior, necrosis, HSP-72 and CLBD up-regulation, and PV down-regulation. Mild or moderate alterations in HSP-72 expression may appear in animals without MRI abnormality.

Neurophysiology

We used extracellular field recordings to assess the integrity of hippocampal physiological function. Similar extracellular granule cell recordings in anesthetized animals have previously been used to assess hippocampal function after repetitive seizure activity, electrical or chemical stimulation (44), and trauma (28). Manipulation of IPI and stimulus frequency permits testing of recurrent inhibition, a measure of network excitability thresholds. The most important physiological finding in our study was that animals that received 60 CGE irradiation or less had normal hippocampal physiology on the irradiated side, whereas animals receiving doses higher than 60 CGE showed altered physiology. Although this finding in an animal model supports the idea that irradiation can alter physiology in epilepsy, the evidence is only indirect in that the animals studied here were naive. A recent study that used rats showed a reduction in seizure activity with significantly lower doses (30). It is possible that less radiation is required to alter the neuronal circuitry in an epileptic animal than in a normal one. Additionally, it is likely that physiological change, like histological and radiographic change, is time-sensitive. It is therefore possible that animals treated with a lower dose

might have displayed physiological changes if sufficient time had elapsed after irradiation.

Physiology on the contralateral side in animals irradiated with 90 CGE and 130 CGE was normal, emphasizing the ability of the proton beam modality to limit irradiation to the intended target. We found that physiology was altered in the 90 CGE animals such that only minimal granule cell spikes were evident, but EPSPs were preserved, albeit at higher-than-normal stimulus voltages. Although this would suggest a reduction in the excitatory threshold of these animals, concomitant loss of recurrent inhibition would speak to the opposite conclusion. These alterations in field potential strength and inhibition observed at higher doses correlate well with necrosis observed on cresyl violet staining, with increased signal on T2-weighted MRI, and with the animals' inability to properly navigate the water maze.

MWM Testing and Visuospatial Memory after PBR

MWM testing was performed to answer two fundamental questions regarding the function of the hippocampus and surrounding neocortex. First, does injury to the unilateral hippocampus and surrounding cortex in the rodent result in visuospatial memory deficit? Second, what relationship exists between physiology, MRI scan appearance, and histology after PBR and the animal's visuospatial memory? Our results strongly support the notion that destruction of one hippocampus in the rodent with associated ipsilateral neocortical injury causes behavioral deficits. This model mimics the damage generated by a temporal lobectomy and hippocampectomy. The dose necessary to impair visual learning via radiosurgery was 90 CGE, a dose that also caused gross histological, radiographic, and physiological compromise of the treated region. Animals receiving 60 CGE or less showed expected learning over the 5-day MWM trial.

Histology after PBR

Histological studies in animals exposed to proton beam irradiation have consistently shown that proton irradiation induces a progressive lesion that, with sufficient dosage and latency, results in cerebral necrosis (1, 14, 22, 24, 31, 33, 39). It is therefore possible that, if we had examined irradiated brains at longer time intervals, even animals receiving lower doses would have displayed histological changes. Although no other studies have documented histology specifically after proton irradiation of the hippocampus, our findings using a Nissl stain were very similar to those of Kondziolka et al. (23), who irradiated the right frontal lobe of rats with the gamma knife and studied them histologically at 3 months. They found necrosis, gliosis, edema, and microhemorrhage in both animals irradiated at 150 Gy and necrosis and astrocytosis in one of two animals irradiated with 100 Gy. Animals that received 70 and 80 Gy displayed shrunken neurons and mild arteriolar thickening, respectively, but animals receiving 60 Gy or less were histologically normal.

Immunocytochemistry after PBR

HSP-72, a member of the 70-kD inducible heat shock protein family, is up-regulated after various insults to the central nervous system, including trauma (7), hyperthermia (2), ischemia (32, 42), and seizure activity (27). It remains unclear whether HSP-72 serves a protective function (2, 49) or is simply a marker of cells undergoing stress that may or may not lead to a cell's death (42, 45). In one experiment, for example, 6 hours of stimulation of the hippocampus via the perforant pathway turned on HSP-72 in the hippocampal dentate gyrus but was insufficient to result in cell death (45). Similarly, in our experiment, HSP-72 was up-regulated after doses of irradiation ranging from 20 to 60 CGE that did not result in cell death, as evidenced by Nissl stain. Gordon et al. (12), however, found that up-regulation of HSP-72 in thymocytes before irradiation protects against apoptotic cell death, suggesting a role for HSP-72 in preventing irradiation-induced cellular injury. In agreement with previous studies that examined HSP-72 regulation after various insults (26, 32, 42), we found HSP-72 to be up-regulated in a graded fashion in response to irradiation dose. Interestingly, the hilus, which has been shown to most readily express HSP-72 in electrical stimulation and ischemia models, was the least inducible cell population after irradiation.

We studied the effects of irradiation on four specific calcium-binding proteins whose localization within specific γ-aminobutyric acid-ergic inhibitory interneurons within the brain have been well characterized in animals and humans in both normal and pathological states (17, 40, 43, 46). In the animals receiving 90 CGE, we found increased staining for CLBD in the dentate gyrus and cortex with abnormal dendritic and cellular architecture restricted to the cortex. No alterations in CLMD, CLRT, or PV were observed at this dose. In the 130 CGE animals, we found abnormal dendritic and cellular architecture in the cortex when staining for CLBD and a decrease in PV in the entorhinal cortex only. This is not surprising, given that the different calcium-binding proteins display selective vulnerabilities in response to other stresses, such as ischemia and seizures. Sloviter et al. (46), for example, in a study of patients with surgically resected hippocampi for intractable temporal lobe epilepsy, found selective survival in cells that expressed PV and CLBD. CLRT-immunoreactive neurons seem to survive in patients with Ammon's horn sclerosis (5, 6). Such findings were confirmed in an electrical stimulation model of epilepsy in the rat (43). Presence of PV and CLBD has similarly conferred resistance to ischemic hippocampal injury in two different rat models of ischemia (11, 18).

Several caveats regarding our immunocytochemical results deserve mention. First, the number of animals in each group was small. We therefore chose to describe the anatomic findings rather than attempt statistical quantitative analysis. Second, because we were interested in correlating the neurophysiology with histology, it was necessary to study brain sections that had minor traumatic contusions from electrode place-

ment. However, this should not have altered the interpretation of results because electrodes were lowered on both sides of the brain and electrode tracks were readily identifiable. Finally, the differences in the calcium-binding proteins within the hippocampus and cortex at higher doses (90 and 130 CGE) must be interpreted with caution because the brains on the irradiated side were quite injured and exhibited significant necrosis. It is not known how this may affect antibody staining irrespective of the true effects from the irradiation.

CONCLUSION

This study describes a new model of stereotactic radiosurgery to the rat hippocampus. We used focused proton beam irradiation of the rat hippocampus to extend our understanding of the radiobiology of radiosurgery by incorporating electrophysiological, immunocytochemical, and behavioral findings. Specifically, necrosis, increased T2 signal, decreased size of granule cell spikes, and impaired ability to perform the MWM were found after 90 CGE at 3 months. Although CLBD was up-regulated in the dentate gyrus and PV was down-regulated in the entorhinal cortex only at necrotic doses, HSP-72 expression was increased at lower nonnecrotic doses.

REFERENCES

1. Andersson B, Larsson B, Leksell L, Mair W, Rexed B, Sourander P, Wennerstrand J: Histopathology of late local radiolesions in the goat brain. **Acta Radiol Ther Phys Biol** 9:385–394, 1970.
2. Barbe MF, Tytell M, Gower DJ, Welch WJ: Hyperthermia protects against light damage in the rat retina. **Science** 241:1817–1820, 1988.
3. Barcia Salorio JL, Roldan P, Hernandez G, Lopez Gomez L: Radiosurgical treatment of epilepsy. **Appl Neurophysiol** 48:400–403, 1985.
4. Blatt DR, Friedman WA, Bova FJ, Theele DP, Mickle JP: Temporal characteristics of radiosurgical lesions in an animal model. **J Neurosurg** 80:1046–1055, 1994.
5. Blumcke I, Beck H, Lie AA, Wiestler OD: Molecular neuropathology of human mesial temporal lobe epilepsy. **Epilepsy Res** 36:205–223, 1999.
6. Blumcke I, Beck H, Nitsch R, Eickhoff C, Scheffler B, Celio MR, Schramm J, Elger CE, Wolf HK, Wiestler OD: Preservation of calretinin-immunoreactive neurons in the hippocampus of epilepsy patients with Ammon's horn sclerosis. **J Neuropathol Exp Neurol** 55:329–341, 1996.
7. Brown IR: Induction of heat shock (stress) genes in the mammalian brain by hyperthermia and other traumatic events: A current perspective. **J Neurosci Res** 27:247–255, 1990.
8. Duan XQ, Wu SL, Li T, Liang JC, Qiou JY, Rao ZR, Ju G: Expression and significance of three types of Fos-immunoreactive cells after gamma knife irradiation of the forebrain in the rat. **Neurosci Res** 33:99–104, 1999.
9. Duan XQ, Wu HX, Liu HL, Rao ZR, Ju G: Expression and changes of Fos protein in the rat forebrain after gamma knife irradiation targeted to the caudate putamen. **Neurosurgery** 45:139–145, 1999.
10. Eisenschenk S, Gilmore RL, Friedman WA, Henchey RA: The effect of LINAC stereotactic radiosurgery on epilepsy associated with arteriovenous malformations. **Stereotact Funct Neurosurg** 71:51–61, 1998.
11. Freund TF, Ylinen A, Miettinen R, Pitkanen A, Lahtinen H, Baimbridge KG, Riekkinen PJ: Pattern of neuronal death in the rat hippocampus after status epilepticus: Relationship to calcium binding protein content and ischemic vulnerability. **Brain Res Bull** 28:27–38, 1992.
12. Gordon SA, Hoffman RA, Simmons RL, Ford HR: Induction of heat shock protein 70 protects thymocytes against radiation-induced apoptosis. **Arch Surg** 132:1277–1282, 1997.
13. Gragoudas ES, Seddon J, Goitein M, Verhey L, Munzenrider J, Urie M, Suit HD, Blitzer P, Koehler A: Current results of proton beam irradiation of uveal melanomas. **Ophthalmology** 92:284–291, 1985.
14. Hassler O: Microangiographic studies on changes in the cerebral vessels after irradiation: Part II—Proton beam lesions in the rat. **Acta Radiol Ther Phys Biol** 4:394–400, 1966.
15. Heikkinen ER, Heikkinen MI, Sotaniemi K: Stereotactic radiotherapy instead of conventional epilepsy surgery: A case report. **Acta Neurochir (Wien)** 119:159–160, 1992.
16. Heikkinen ER, Konnov B, Melnikov L, Yalynych N, Zubkov Y, Garmashov Y, Pak VA: Relief of epilepsy by radiosurgery of cerebral arteriovenous malformations. **Stereotact Funct Neurosurg** 53:157–166, 1989.
17. Hof PR, Glezer II, Conde F, Flagg RA, Rubin MB, Nimchinsky EA, Vogt Weisenhorn DM: Cellular distribution of the calcium-binding proteins parvalbumin, calbindin, and calretinin in the neocortex of mammals: Phylogenetic and developmental patterns. **J Chem Neuroanat** 16:77–116, 1999.
18. Hsu M, Sik A, Gallyas F, Horvath Z, Buzsaki G: Short-term and long-term changes in the postischemic hippocampus. **Ann N Y Acad Sci** 743:121–139, 1994.
19. Kamiryo T, Berr SS, Berk HW, Lee KS, Kassell NF, Steiner L: Accuracy of an experimental stereotactic system for MRI-based gamma knife irradiation in the rat. **Acta Neurochir (Wien)** 138:1103–1107, 1996.
20. Kamiryo T, Kassell NF, Thai QA, Lopes MB, Lee KS, Steiner L: Histological changes in the normal rat brain after gamma irradiation. **Acta Neurochir (Wien)** 138:451–459, 1996.
21. Karger CP, Hartman GH, Hoffmann U, Lorenz WJ: A system for stereotactic irradiation and magnetic resonance evaluations in the rat brain. **Int J Radiat Oncol Biol Phys** 33:485–492, 1995.
22. Kennedy AS, Archambeau JO, Archambeau MH, Holshouser B, Thompson J, Moyers M, Hinshaw D Jr, Slater JM: Magnetic resonance imaging as a monitor of changes in the irradiated rat brain: An aid in determining the time course of events in a histologic study. **Invest Radiol** 30:214–220, 1995.
23. Kondziolka D, Lunsford LD, Claassen D, Maitz AH, Flickinger JC: Radiobiology of radiosurgery: Part I—The normal rat brain model. **Neurosurgery** 31:271–279, 1992.
24. Larsson B, Leksell L, Rexed B, Sourander P, Mair W, Andersson B: The high-energy proton beam as a neurosurgical tool. **Nature** 182:1222–1223, 1958.
25. Lo EH, Frankel KA, Steinberg GK, DeLaPaz RL, Fabrikant JI: High-dose single-fraction brain irradiation: MRI, cerebral blood flow, electrophysiological, and histological studies. **Int J Radiat Oncol Biol Phys** 22:47–55, 1992.
26. Lowenstein DH, Chan PH, Miles MF: The stress protein response in cultured neurons: Characterization and evidence for a protective role in excitotoxicity. **Neuron** 7:1053–1060, 1991.
27. Lowenstein DH, Simon RP, Sharp FR: The pattern of 72-kDa heat shock protein-like immunoreactivity in the rat brain following flurothyl-induced status epilepticus. **Brain Res** 531:173–182, 1990.
28. Lowenstein DH, Thomas MJ, Smith DH, McIntosh TK: Selective vulnerability of dentate hilar neurons following traumatic brain injury: A potential mechanistic link between head trauma and disorders of the hippocampus. **J Neurosci** 12:4846–4853, 1992.
29. Manlapaz JS, Astrom KE, Ballantine HT, Lele PP: Effects of ultrasonic radiation in experimental focal epilepsy in the cat. **Exp Neurol** 10:345–356, 1964.
30. Mori Y, Kondziolka D, Balzer J, Fellows W, Flickinger JC, Lunsford LD, Thulborn KR: Effects of stereotactic radiosurgery on an animal model of hippocampal epilepsy. **Neurosurgery** 46:157–165, 2000.
31. Nielsen SL, Kjellberg RN, Asbury AK, Koehler AM: Neuropathologic effects of proton-beam irradiation in man: Part II—Evaluation after pituitary irradiation. **Acta Neuropathol (Berl)** 21:76–82, 1972.
32. Nowak TS Jr, Bond U, Schlesinger MJ: Heat shock RNA levels in brain and other tissues after hyperthermia and transient ischemia. **J Neurochem** 54: 451–458, 1990.
33. Omary RA, Berr SS, Kamiryo T, Lanzino G, Kassell NF, Lee KS, Lopes MB, Hillman BJ: 1995 AUR Memorial Award: Gamma knife irradiation-induced changes in the normal rat brain studied with 1H magnetic resonance spectroscopy and imaging. **Acad Radiol** 2:1043–1051, 1995.
34. Paxinos G, Watson C: *The Rat Brain in Stereotaxic Coordinates*. San Diego, Academic Press, 1986.

35. Reder CS, Moyers MF, Lau D, Kirby MA: Studies of physiology and the morphology of the cat LGN following proton irradiation. **Int J Radiat Oncol Biol Phys** 46:1247–1257, 2000.
36. Regis J, Bartolomei F, Metellus P, Rey M, Genton P, Dravet C, Bureau M, Semah F, Gastaut JL, Peragut JC, Chauvel P: Radiosurgery for trigeminal neuralgia and epilepsy. **Neurosurg Clin N Am** 10:359–377, 1999.
37. Regis J, Bartolomei F, Rey M, Genton P, Dravet C, Semah F, Gastaut JL, Chauvel P, Peragut JC: Gamma knife surgery for mesial temporal lobe epilepsy. **Epilepsia** 40:1551–1556, 1999.
38. Regis J, Kerkerian-Legoff L, Rey M, Vial M, Porcheron D, Nieoullon A, Peragut JC: First biochemical evidence of differential functional effects following Gamma Knife surgery. **Stereotact Funct Neurosurg** 66[Suppl 1]:29–38, 1996.
39. Rexed B, Mair W, Sourander P, Larsson B, Leksell L: Effect of high energy protons on the brain of the rabbit. **Acta Radiol** 53:289–299, 1959.
40. Rogers J, Khan M, Ellis J: Calretinin and other CaBPs in the nervous system. **Adv Exp Med Biol** 269:195–203, 1990.
41. Rogers M, Myers R, Jenkinson T, Hornsey S: Histology of the irradiated rat brain in the first post-irradiation year. **Br J Radiol** 55:208–212, 1982.
42. Simon RP, Cho H, Gwinn R, Lowenstein DH: The temporal profile of 72-kDa heat-shock protein expression following global ischemia. **J Neurosci** 11:881–889, 1991.
43. Sloviter RS: Calcium-binding protein (calbindin-D28k) and parvalbumin immunocytochemistry: Localization in the rat hippocampus with specific reference to the selective vulnerability of hippocampal neurons to seizure activity. **J Comp Neurol** 280:183–196, 1989.
44. Sloviter RS: Possible functional consequences of synaptic reorganization in the dentate gyrus of kainate-treated rats. **Neurosci Lett** 137:91–96, 1992.
45. Sloviter RS, Lowenstein DH: Heat shock protein expression in vulnerable cells of the rat hippocampus as an indicator of excitation-induced neuronal stress. **J Neurosci** 12:3004–3009, 1992.
46. Sloviter RS, Sollas AL, Barbaro NM, Laxer KD: Calcium-binding protein (calbindin-D28K) and parvalbumin immunocytochemistry in the normal and epileptic human hippocampus. **J Comp Neurol** 308:381–396, 1991.
47. Sun B, DeSalles AA, Medin PM, Solberg TD, Hoebel B, Felder-Allen M, Krahl SE, Ackermann RF: Reduction of hippocampal-kindled seizure activity in rats by stereotactic radiosurgery. **Exp Neurol** 154:691–695, 1998.
48. Warnke PC, Berlis A, Weyerbrock A, Ostertag CB: Significant reduction of seizure incidence and increase of benzodiazepine receptor density after interstitial radiosurgery in low-grade gliomas. **Acta Neurochir Suppl (Wien)** 68:90–92, 1997.
49. Welch WJ: The mammalian heat shock (or stress) response: A cellular defense mechanism. **Adv Exp Med Biol** 225:287–304, 1987.

Acknowledgments

We thank Ethan W. Cascio for technical assistance with proton beam irradiation, Patricia L. Lee, Ph.D., for technical assistance with MRI, Marek Ancukiewicz, Ph.D., for statistical assistance, Christina T. Shay for assistance with the MWM, and David Feliciano for assistance with figure preparation. We also thank Nicholas T. Zervas, M.D., and Jay S. Loeffler, M.D., for critical analysis of this work and their encouragement to pursue this area of research. This work was supported by a fellowship grant from the Center for Innovative Minimally Invasive Therapy (to JLB) and Grant NS036224 from the National Institute of Neurological Disorders and Stroke (to AJC).

COMMENTS

The authors have evaluated the effects of proton beam radiosurgery on the normal rat hippocampus. They found that radiosurgical doses at 90 or 130 Gy led to frank tissue necrosis and associated imaging changes. Behavior changes also were noted with those doses. At a dose of 60 Gy or less, no histological or behavior changes were noted. This work supports findings at my laboratory (1, 2). It seems that in the rat brain, small-volume radiosurgery leads to tissue necrosis at doses at or higher than 100 Gy during a period of 3 months. Lower doses do not. Specifically, my colleagues and I have tested the effects of doses between 20 and 60 Gy in the rat hippocampus without any evidence of behavior, imaging, or histological changes. What is the clinical value of this information? Radiosurgery may prove to be an effective alternative treatment to surgical resection for lesional epilepsy. The goal of radiosurgery is to treat the epileptic focus but spare normal brain or regional brain function. At a nonnecrotizing dose, the hope is that epilepsy can be controlled without significant morbidity from removal or exposure of brain tissue. In our rat hippocampal radiosurgery model, we found that doses of 30 or 60 Gy did lead to the cessation of seizures and that cessation was achieved without behavior or histological problems. The effects of radiosurgery on mesial temporal lobe sclerosis in humans are currently being tested in a multicenter randomized trial.

Douglas Kondziolka
Pittsburgh, Pennsylvania

---

1. Maesawa S, Kondziolka D, Dixon CE, Balzer J, Fellows W, Lunsford LD: Subnecrotic stereotactic radiosurgery controlling epilepsy produced by kainic acid injection in rats. **J Neurosurg** 93:1033–1040, 2000.
2. Mori Y, Kondziolka D, Balzer J, Fellows W, Flickinger JC, Lunsford LD, Thulborn KR: Effects of stereotactic radiosurgery on an animal model of hippocampal epilepsy. **Neurosurgery** 46:157–168, 2000.

The authors have studied some of the behavioral, anatomic, and physiological effects of proton beam radiosurgery delivered to the rat hippocampus. They clearly demonstrate that aberrations of all these effects occur at about a 60-cobalt-Gray-equivalent threshold. Of interest is the greater sensitivity of heat shock protein expression, implying that more subtle alterations in physiology might occur at nonnecrotizing doses of radiation. I presume that this work is a prelude to testing the effectiveness of this technique in a hippocampus-based seizure model. This work will be an important baseline against which to judge the potential mechanisms involved in radiation-based seizure control. The data presented here are clear, and the conclusions are justified. The relative precision of proton beam radiation compared with more commonly used LINAC- or cobalt-based methods is of great importance regarding the interpretation of these results and their applicability to current studies of radiation treatment for patients with medial temporal sclerosis and related seizure disorders.

Charles J. Hodge, Jr.
Syracuse, New York

Gamma knife radiosurgery has been proposed as an alternative treatment modality for patients with temporal lobe epilepsy due to hippocampal sclerosis. Although initial reports showed promising results, there has been a significant lack of understanding of the electrophysiological, behavior, imaging, cellular, and molecular changes associated with and after radiosurgery using various radiation doses. Brisman et al. systematically address these issues. The importance of this

report lies in the fact that it expands understanding of the effects of radiosurgery on the rodent brain. Further studies designed to correlate the various findings with in vivo electroencephalography in animal models of limbic seizures should complement these results and, I hope, improve understanding of the potential utility and side effects of and the indications for radiosurgery as a treatment modality for patients with temporal lobe epilepsy.

Hans O. Lüders
Imad Najm
Neurologists
Cleveland, Ohio

The authors point out that the use of radiosurgery has increased greatly in recent years but that little is known of the effects on brain function of clinically used doses of radiation, which do not cause frank brain tissue necrosis but may modify function. The authors bring a wide range of techniques to bear on this question and demonstrate that rat hippocampal structure and function are preserved at doses of up to 60 cobalt Gray equivalents. However, heat shock protein 72, a protein thought to have a protective role, is increased at doses of 20 to 60 cobalt Gray equivalents.

Robert G. Grossman
Houston, Texas

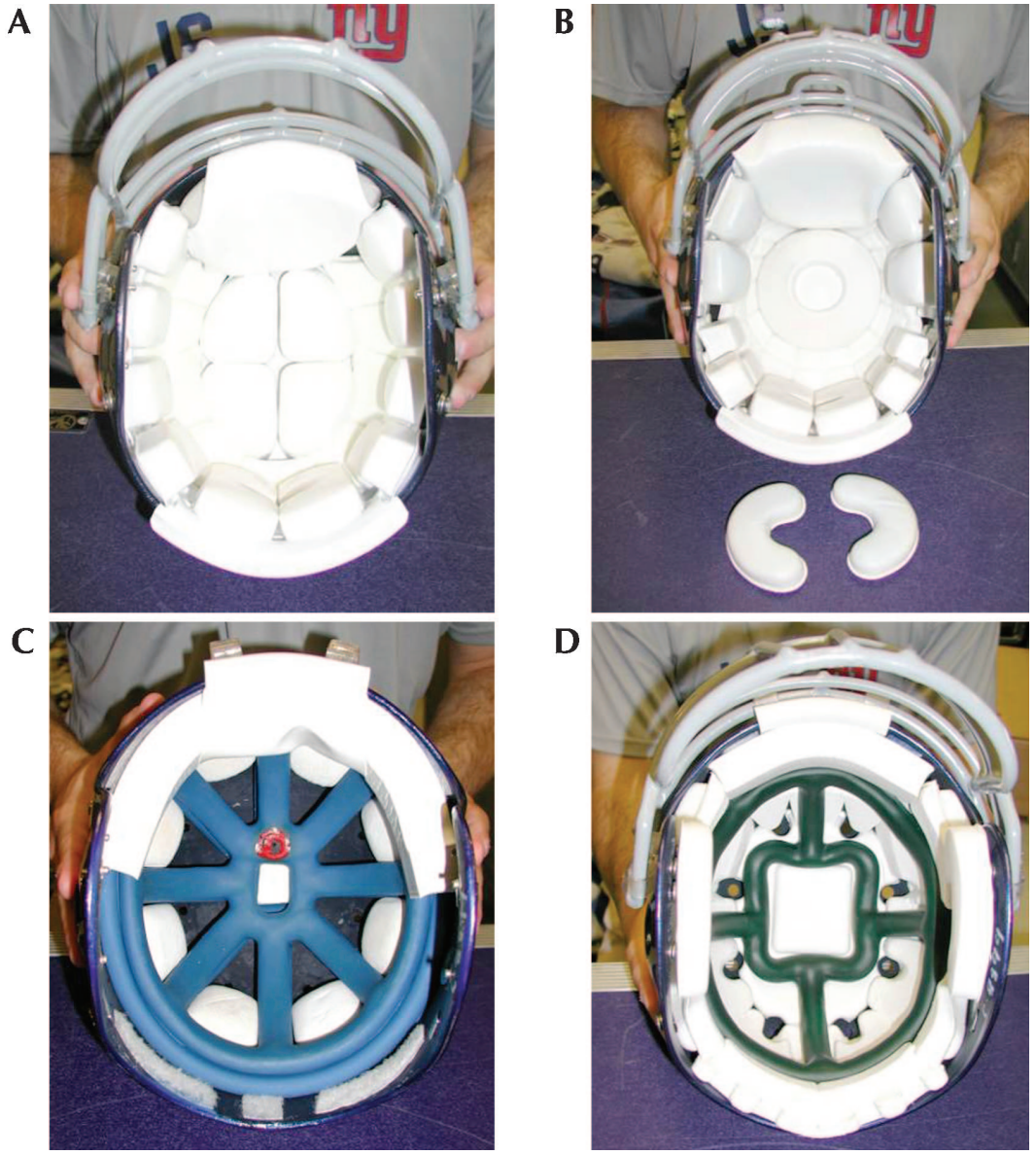

Modern helmet configurations. A *and* B, *inner compartment showing foam components and size variables. Foam inserts may be varied according to the cranial contour.* C, *inner compartment of a double-chamber pneumatic crown system. The outer crown is fully inflated, and the inner crown is inflated to fit; shell and foam inserts may be varied in relation to cranial contour needs.* D, *Schutt lightweight helmet system. Currently, this system is widely available only in professional level competition. Its innovative air crown system, with multisectional foam components, offers complete contour fitting to multivariable cranial contours and proportions. The helmet, combined with a titanium base frame mask, offers a reduction in helmet weight of more than 30% (also see p. 972). (Courtesy, Joseph Skiba and the New York Football Giants.)*